ANTENNA PATTERN CONTROL USING IMPEDANCE SURFACES

Semiannual Progress Report

Constantine A. Balanis and Kefeng Liu

September 16, 1990 - March 15, 1991

Telecommunication Research Center
Department of Electrical Engineering
Arizona State University
Tempe, Arizona 85287-7206

Grant No. NAG-1-1183
National Aeronautics and Space Administration
Joint Research Program Office
Langley Research Center
Hampton, VA 23665

ANTENNA PATTERN CONTROL USING IMPEDANCE SURFACES

Semiannual Progress Report

Constantine A. Balanis and Kefeng Liu

September 16, 1990 - March 15, 1991

Telecommunication Research Center
Department of Electrical Engineering
Arizona State University
Tempe, Arizona 85287-7206

Grant No. NAG-1-1183
National Aeronautics and Space Administration
Joint Research Program Office
Langley Research Center
Hampton, VA 23665

ABSTRACT

This is a semiannual progress report for the *Antenna Pattern Control Using Impedance Surfaces* research grant. This report covers the research period from September 16, 1990 to March 15, 1991.

During this research period, a design method for selecting a low-loss impedance material coating for a horn antenna pattern control has been developed. This method and the stepped waveguide technique can be employed to accurately compute the electromagnetic wave phenomenon inside the transition region of the horn antenna, with or without the impedance surfaces, from the feed to the radiating aperture. For moment method solutions of the electric and magnetic current distributions on the radiating aperture and the outer surface of the horn antenna, triangular surface-patch modes are introduced to replace the sinusoidal surface-patch modes as expansion and testing functions to provide a more physical expansion of the current ditributions.

In the synthesis problem, a numerical optimization process is formulated to minimize the error function between the desired waveguide modes and the modes provided by the horn transition with impedance surfaces. Since the modes generated by the horn transition with impedance surface are computed by analytical techniques, the computational error involved in the synthesis of the antenna pattern is minimum. Therefore, the instability problem can be avoided.

A preliminary implementation of the techniques has demonstrated that the developed theory of the horn antenna pattern control using the impedance surfaces is realizable.

I. INTRODUCTION

As a continuity of the last reporting period, the research of this reporting period has concentrated on the problems encountered in the previous period. New approaches and alternative solutions have been found and developed. In this section, each problem and its solution are presented in detail.

A. Stepped Waveguide Technique

In the previous reporting period, we have indicated a need for an alternative solution to the variable-dependent first order differential equations formulated to compute the transition taper of a perfectly conducting horn. A comprehensive study of the alternative solution has been conducted. As examined by [1] and [2], the numerical technique in solving the first order differential equation yields the same results as given by the stepped-waveguide technique [3,4,5,6] when the size of the steps is sufficiently small. A numerical solution of the differential equation must also be performed with a finite advancing step size, and due to the numerical problem caused by evanescent modes, the taper has to be divided into several sections. The hybrid matrix of each section needs to be computed separately, and translated and combined into a scattering matrix. Such a technique is inconvenient for a horn with impedance surfaces and for the numerical optimization process in the synthesis problem. On the other hand, the stepped-waveguide technique utilizes a finite number of subdivisions of waveguide steps to approach the continuous horn taper. Within each waveguide step, the waveguide section is uniform. The scattering matrices of each individual waveguide step are related to each other by the electromagnetic boundary conditons on the discontinuous junctions connecting them. The combination of the scattering

matrices of all the steps gives the total scattering matrix of the horn transition. Such a method is very convenient to be extended to compute the scattering matix of a horn transition with impedance surfaces and to be compatible with optimization process in the synthesis problem. As indicated in [1] for the circular waveguide taper case, the computation time for the two techniques is about the same. Therefore, in our application, the stepped-waveguide technique is an ideal alternative to compute the scattering matrix of a horn transition. In the next section, we will briefly describe the stepped-waveguide technique, especially as developed for modeling to the horn transition with impedance walls.

1. Scattering Matrix of a Stepped Waveguide

By using the full-wave expansion technique, a field distribution on a section of waveguide can be expanded as the superposition of all possible modes. For a rectangular waveguide, instead of representing the field distributions by using TM_z and TE_z as performed in [3]-[6], it is more convenient to use the cross-sectional components of the vector potential to characterize the eigenmodes. If we choose TM_y and TE_y modes, the field inside a rectangular waveguide can be expressed in terms of A_y and F_y. For perfectly conducting surfaces, the two components of the vector potential can be written as

$$A_y = j\mu \sum_{mn} (A_{mn} e^{-j\beta_z z} + B_{mn} e^{j\beta_z z}) S_{mn}(x,y) \tag{1}$$

$$F_y = j\epsilon \sum_{mn} (C_{mn} e^{-j\beta_z z} - D_{mn} e^{j\beta_z z}) T_{mn}(x,y) \tag{2}$$

$$S_{mn}(x,y) = \frac{2\sin(\beta_x x)\cos(\beta_y y)}{\sqrt{ab(1+\delta_{no})}} \tag{3}$$

$$T_{mn}(x,y) = \frac{2\cos(\beta_x x)\sin(\beta_y y)}{\sqrt{ab}} \tag{4}$$

Then the electric and magnetic fields due to the vector potential can be found by the following equations:

$$E_x = -j\frac{1}{\omega\mu\epsilon}\frac{\partial^2 A_y}{\partial x \partial y} + \frac{1}{\epsilon}\frac{\partial F_y}{\partial z} \tag{5}$$

$$E_y = -j\frac{1}{\omega\mu\epsilon}(\omega^2\mu\epsilon + \frac{\partial^2 A_y}{\partial^2 y})A_y \tag{6}$$

$$E_z = -j\frac{1}{\omega\mu\epsilon}\frac{\partial^2 A_y}{\partial z \partial y} - \frac{1}{\epsilon}\frac{\partial F_y}{\partial x} \tag{7}$$

and

$$H_x = -\frac{1}{\mu}\frac{\partial A_y}{\partial z} - j\frac{1}{\omega\mu\epsilon}\frac{\partial^2 F_y}{\partial x \partial y} \tag{8}$$

$$H_y = -j\frac{1}{\omega\mu\epsilon}(\omega^2\mu\epsilon + \frac{\partial^2 F_y}{\partial^2 y})F_y \tag{9}$$

$$H_z = \frac{1}{\mu}\frac{\partial A_y}{\partial x} - j\frac{1}{\omega\mu\epsilon}\frac{\partial^2 F_y}{\partial z \partial y} \tag{10}$$

Therefore, the full-wave expansion of the fields can be expressed as

$$E_x|_{z=0} = \sum_{mn}[\beta_z(C_{mn} + D_{mn}) - \frac{\beta_x\beta_y}{\omega\epsilon}(A_{mn} + B_{mn})]T_{mn}(x,y) \tag{11}$$

$$E_y|_{z=0} = \frac{1}{\omega\epsilon}\sum_{mn}(\omega^2\mu\epsilon - \beta_y^2)(A_{mn} + B_{mn})S_{mn}(x,y) \tag{12}$$

$$H_x|_{z=0} = -\sum_{mn}[\frac{\beta_x\beta_y}{\omega\mu}(C_{mn} - D_{mn}) + \beta_z(A_{mn} - B_{mn})]S_{mn}(x,y) \tag{13}$$

$$H_y|_{z=0} = \frac{1}{\omega\mu}\sum_{mn}(\omega^2\mu\epsilon - \beta_y^2)(C_{mn} - D_{mn})T_{mn}(x,y) \tag{14}$$

When there is a discontinuous junction at $z = 0$, the boundary conditions correlating the two waveguides are

$$E^{(1)}(x,y)|_{onA} = E^{(2)}(x,y)|_{onA} \tag{15}$$

$$E^{(2)}(x,Y)|_{on\Delta A} = 0 \tag{16}$$

$$H^{(1)}(x,y)|_{onA} = H^{(2)}(x,y)|_{onA} \tag{17}$$

where A is the area of the smaller waveguide section. The boundary conditions in (15)-(17) provide the same number of equations as the number of the amplitude coefficients in the full-wave expansion. This establishes a unique correspondance between the full-wave exapnsion coefficients on both sides. Therefore, the relationships between the full-wave expansion coefficients on both side of the waveguide can be found by

$$\beta_z^{(2)}(C_{mn}^{(2)} + D_{mn}^{(2)}) - \frac{\beta_x^{(2)}\beta_y^{(2)}}{\omega\epsilon}(A_{mn}^{(2)} + B_{mn}^{(2)}) =$$

$$\sum_{kl}[\beta_z^{(1)}(C_{kl}^{(1)} + D_{kl}^{(1)}) - \frac{\beta_x^{(1)}\beta_y^{(1)}}{\omega\epsilon}(A_{kl}^{(1)} + B_{kl}^{(1)})]V_{mnkl} \tag{18}$$

$$(\omega^2\mu\epsilon - \beta_y^{(2)^2})(A_{mn}^{(2)} + B_{mn}^{(2)}) = \sum_{kl}(\omega^2\mu\epsilon - \beta_y^{(1)^2})(A_{kl}^{(1)} + B_{kl}^{(1)})U_{mnkl} \tag{19}$$

$$\beta_z^{(1)}(A_{kl}^{(1)} - B_{kl}^{(1)}) + \frac{\beta_x^{(1)}\beta_y^{(1)}}{\omega\mu}(C_{kl}^{(1)} - D_{kl}^{(1)}) =$$

$$\sum_{mn}[\beta_z^{(2)}(A_{mn}^{(2)} - B_{mn}^{(2)}) + \frac{\beta_x^{(2)}\beta_y^{(2)}}{\omega\mu}(C_{mn}^{(2)} - D_{mn}^{(2)})]U_{mnkl} \tag{20}$$

$$(\omega^2\mu\epsilon - \beta_y^{(1)^2})(C_{kl}^{(1)} - D_{kl}^{(1)}) = \sum_{mn}(\omega^2\mu\epsilon - \beta_y^{(2)^2})(C_{mn}^{(2)} - D_{mn}^{(2)})V_{mnkl} \tag{21}$$

where

$$U_{mnkl} = \frac{4\int_0^{a_1}\int_0^{b_1}\sin(\beta_x^{(2)}x')\sin(\beta_x^{(1)}x)\cos(\beta_y^{(2)}y')\cos(\beta_y^{(1)}y)dxdy}{\sqrt{a_1a_2b_1b_2(1+\delta_{no})(1+\delta_{lo})}} \tag{22}$$

$$V_{mnkl} = \frac{4\int_0^{a_1}\int_0^{b_1}\cos(\beta_x^{(2)}x')\cos(\beta_x^{(1)}x)\sin(\beta_y^{(2)}y')\sin(\beta_y^{(1)}y)dxdy}{\sqrt{a_1a_2b_1b_2}} \tag{23}$$

$$x' = x + \frac{\Delta a}{2} = x + \frac{a_2 - a_1}{2} \tag{24}$$

$$y' = y + \frac{\Delta b}{2} = y + \frac{b_2 - b_1}{2} \tag{25}$$

For perfectly conducting waveguide walls, the integration and U_{mnkl} and V_{mnkl} are

given analytically by

$$U_{mnkl} = \frac{4[1+(-1)^{m+k}][1+(-1)^{n+l}]\beta_x^{(1)}\beta_y^{(2)}\sin(\beta_x^{(2)}\frac{\Delta a}{2})\cos(\beta_y^{(2)}\frac{\Delta b}{2})}{\sqrt{a_1 a_2 b_1 b_2(1+\delta_{no})(1+\delta_{lo})}} \tag{26}$$

$$V_{mnkl} = \frac{\beta_x^{(2)}\beta_y^{(1)}}{\beta_x^{(1)}\beta_y^{(2)}} U_{mnkl} \tag{27}$$

Doing some tedious but straight forward manipulations of the boundary condition equations, the relation of the full-wave expansion coefficients on both sides of the junction can be expressed by

$$A_{mn}^{(2)} + B_{mn}^{(2)} = \sum_{kl} \frac{\omega^2\mu\epsilon - {\beta_y^{(1)}}^2}{\omega^2\mu\epsilon - {\beta_y^{(2)}}^2}(A_{kl}^{(1)} + B_{kl}^{(1)})]U_{mnkl} \tag{28}$$

$$\begin{aligned} C_{mn}^{(2)} + D_{mn}^{(2)} &= \sum_{kl} \frac{\omega\mu\beta_x^{(2)}({\beta_y^{(2)}}^2 - {\beta_y^{(1)}}^2)}{\beta_z^{(2)}\beta_y^{(2)}(\omega^2\mu\epsilon - {\beta_y^{(2)}}^2)} U_{mnkl}(A_{kl}^{(1)} + B_{kl}^{(1)}) \\ &+ \sum_{kl} \frac{\beta_z^{(1)}}{\beta_z^{(2)}} V_{mnkl}(C_{kl}^{(1)} + D_{kl}^{(1)}) \end{aligned} \tag{29}$$

$$\begin{aligned} A_{kl}^{(1)} - B_{kl}^{(1)} &= \sum_{mn} \frac{\beta_z^{(2)}}{\beta_z^{(1)}} U_{mnkl}(A_{mn}^{(2)} - B_{mn}^{(2)}) \\ &+ \sum_{mn} \frac{\omega\epsilon\beta_x^{(2)}({\beta_y^{(2)}}^2 - {\beta_y^{(1)}}^2)}{\beta_z^{(1)}\beta_y^{(2)}(\omega^2\mu\epsilon - {\beta_y^{(1)}}^2)} U_{mnkl}(C_{mn}^{(2)} - D_{mn}^{(2)}) \end{aligned} \tag{30}$$

$$C_{kl}^{(1)} - D_{kl}^{(1)} = \sum_{mn} \frac{\omega^2\mu\epsilon - {\beta_y^{(2)}}^2}{\omega^2\mu\epsilon - {\beta_y^{(1)}}^2}(C_{mn}^{(2)} - D_{mn}^{(2)})]V_{mnkl} \tag{31}$$

To express (28)-(31) in matrix form, let

$$a^{(1)} = \begin{pmatrix} A_{kl}^{(1)} \\ C_{kl}^{(1)} \end{pmatrix} \qquad b^{(1)} = \begin{pmatrix} B_{kl}^{(1)} \\ D_{kl}^{(1)} \end{pmatrix} \tag{32}$$

$$a^{(2)} = \begin{pmatrix} A_{mn}^{(2)} \\ C_{mn}^{(2)} \end{pmatrix} \qquad b^{(2)} = \begin{pmatrix} B_{mn}^{(2)} \\ D_{mn}^{(2)} \end{pmatrix} \tag{33}$$

Then, the matrix equations of (28)-(31) are

$$a^{(2)} + b^{(2)} = Y(a^{(1)} + b^{(1)}) \tag{34}$$

$$a^{(1)} - b^{(1)} = Z(a^{(2)} - b^{(2)}) \tag{35}$$

where Y is a matrix with corresponding elements defined by equations (28) and (29), and Z by (30) and (31), respectively. With a simple mathematical manipulation of the two matrix equations, the scattering matrix of the stepped waveguide junction can be obtained in the form of

$$\begin{pmatrix} b^{(1)} \\ a^{(2)} \end{pmatrix} = \begin{pmatrix} (I+ZY)^{-1}(I-ZY) & 2(I+ZY)^{-1}Z \\ 2(I+YZ)^{-1}Y & (I+YZ)^{-1}(YZ-I) \end{pmatrix} \begin{pmatrix} a^{(1)} \\ b^{(2)} \end{pmatrix} \tag{36}$$

2. Combination of the Stepped Scattering Matrices

Consider two series stepped waveguide each having the scattering matrix of the form

$$\begin{pmatrix} b^{(i)} \\ a^{(i+1)} \end{pmatrix} = \begin{pmatrix} S_{11}^{(i)} & S_{12}^{(i)} \\ S_{21}^{(i)} & S_{22}^{(i)} \end{pmatrix} \begin{pmatrix} a^{(i)} \\ b^{(i+1)} \end{pmatrix} \tag{37}$$

$$\begin{pmatrix} b^{(i+1)} \\ a^{(i+2)} \end{pmatrix} = \begin{pmatrix} S_{11}^{(i+1)} & S_{12}^{(i+1)} \\ S_{21}^{(i+1)} & S_{22}^{(i+1)} \end{pmatrix} \begin{pmatrix} a^{(i+1)} \\ b^{(i+2)} \end{pmatrix} \tag{38}$$

where the scattering matrices in the i-th and (i+1)-th section of stepped waveguides are given by the combination of their junction scattering matrices and the corresponding propagation matrices due to the lengths of the waveguide section. They can be expressed as

$$S_{11}^{(\nu)} = [I + Z^{(\nu)}Y^{(\nu)}]^{-1}[I - Z^{(\nu)}Y^{(\nu)}] \tag{39}$$

$$S_{12}^{(\nu)} = 2[I + Z^{(\nu)}Y^{(\nu)}]^{-1}Z^{(\nu)}D^{(\nu)} \tag{40}$$

$$S_{21}^{(\nu)} = 2D^{(\nu)}[I + Y^{(\nu)}Z^{(\nu)}]^{-1}Y^{(\nu)} \tag{41}$$

$$S_{22}^{(\nu)} = D^{(\nu)}[I + Y^{(\nu)}Z^{(\nu)}]^{-1}[Y^{(\nu)}Z^{(\nu)} - I]D^{(\nu)} \tag{42}$$

where the propagation matix $D^{(\nu)}$ is a diagonal matrix expressing the phase delay or magnitude attenuation of all possible positively going modes in the full-wave expansion of the ν-th (i-th or (i+1)-th) section of the waveguide which has a length of $d^{(\nu)}$. The elment of $D^{(\nu)}$ is given by

$$D_{kk}^{(\nu)} = e^{-j\beta_k^{(\nu)} d^{(\nu)}} \tag{43}$$

Using (37) and (38), one can expand the two scattering matrices and obtain the combined scattering matrix of

$$\begin{pmatrix} b^{(i)} \\ a^{(i+2)} \end{pmatrix} = \begin{pmatrix} S_{11}^{(comb)} & S_{12}^{(comb)} \\ S_{21}^{(comb)} & S_{22}^{(comb)} \end{pmatrix} \begin{pmatrix} a^{(i)} \\ b^{(i+2)} \end{pmatrix} \tag{44}$$

where

$$S_{11}^{(comb)} = S_{11}^{(i)} + S_{12}^{(i)} F S_{11}^{(i+1)} S_{21}^{(i)} \tag{45}$$

$$S_{12}^{(comb)} = S_{12}^{(i)} F S_{12}^{(i+1)} \tag{46}$$

$$S_{21}^{(comb)} = S_{21}^{(i+1)} G S_{21}^{(i)} \tag{47}$$

$$S_{22}^{(comb)} = S_{22}^{(i+1)} + S_{21}^{(i+1)} G S_{22}^{(i)} S_{12}^{(i+1)} \tag{48}$$

with

$$F = [I - S_{11}^{(i+1)} S_{22}^{(i)}]^{-1} \tag{49}$$

$$G = [I - S_{22}^{(i)} S_{11}^{(i+1)}]^{-1} \tag{50}$$

The computer program development of scattering matrices for stepped waveguides and the combined scattering matrix for the total horn transition has been fully accomplished.

3. Horn Transition with Impedance Surfaces

The coating of lossy materials on the walls of the horn antenna introduces a change of the electromagnetic field distribution along the horn transition. Technically, it is important to point out that the symmetry of the coating is very important because the asymmetry will introduce a significant cross polarization as noted in [7]. Figure 1 shows the geometry of an H-plane coated horn transition and its stepped waveguide model. The difference between the coated and uncoated stepped waveguide section is the eigenfunctions in the full-wave expansions. To find the new eigenfunctions, we start with the search for the new eigenvalues for each individual eigenfunction based on the boundary conditions across the surfaces of the coating material. Such a process can be emulated by using the Transverse Resonance Method(TRM)[8] when coatings are applied on the top and the bottom walls, and TM_y and TE_y modes are used to represent the field distribution. By using the TRM technique, the cross-sectional wave constants can be obtained by solving the following two complex transcedental equations for TE_y and TM_y modes, respectively:

$$\frac{\beta_e}{\epsilon_d}\tan(\beta_e h) + \beta_{oe}\tan(\beta_{oe} d) = 0 \qquad {\beta_e}^2 - {\beta_{oe}}^2 = \omega^2\mu_o\epsilon_o(\mu_r\epsilon_r - 1) \tag{51}$$

$$\frac{\beta_m}{\mu_d}\cot(\beta_m h) + \beta_{om}\cot(\beta_{om} d) = 0 \qquad {\beta_m}^2 - {\beta_{om}}^2 = \omega^2\mu_o\epsilon_o(\mu_r\epsilon_r - 1) \tag{52}$$

where (β_e, β_{oe}), and (β_m, β_{om}) are the complex propagation constants inside and outside the coating material for TE_y and TM_y modes, respectively. The solution of (51) and (52) requires a dedicated complex root solver in order not to miss any root in the complete eigenvalue sequence. Such a complex root solver has been developed in this research period. Once the complex eigenvalues are provided, the scattering matrix

for each individual coated waveguide step can be found following similar procedures as that of the perfectly conducting waveguide step presented earlier. The technique of combining the scattering matrices of the coated waveguide steps is identical to that of the uncoated case.

When the change of electromagnetic field distribution introduced by the lossy material coating is computed by using the corresponding complex eigenfunctions, the results are analytical. Therefore, the effects of impedance surfaces are computed more accurately using this precedure than by using the approximated impedance boundary condition. The lack of stability encountered when solving the synthesis problem in the previous research period can be sucessfully circumvented.

B. Development in Moment Method Solution

Since all of the inside surfaces of the horn transition with or without the impedance surfaces has been analyzed by the stepped waveguide technique, the momemt method is applied only to solve for the electric and magnetic current distributions on the radiating aperture and the outer surface of the antenna. Previous studies have indicated a need to include the outer surface of the antenna in the Moment Method solution in order to predict accurately the radiation pattern in the back region. The rapid variant ripples in the H-plane radiation pattern are due to the electric currents excited on the outside surface of the horn. In this research period, significant efforts were expanded to include part or all of the outer surface.

When the outer surfaces of the horn antenna are included in the moment method solution, a large number of unknowns are introduced in the hybrid matrix equation. Therefore, there is a need for a more physical expansion and testing modes to allow accurate field computation with a largest possible element size. Figure 2 demonstrates

an accuracy comparison of the function expansion of a typical aperture current distribution mode $\sin(\frac{\pi x}{a})$ with a Galerkin testing using the subsectional sinusoidal and triangular functions. The segment size is 0.25λ, which is the maximum segment size for the subsectional sinusoidal mode. Figure 2 clearly indicates that the triangular subsectional function out-performs the subsectional sinusoidal function in providing an accurate expansion of the current ditributions with a relatively large segment size. Therefore, the triangular surface-patch function (or roof-top function) has been chosen to be the expansion and testing function in the moment method solution. The coding of the impedance elements between the electric and electric modes has been developed and proven to be very efficient. The coding of the impedance element between electric and magnetic modes will soon be completed.

C. Low-Loss Design using Impedance Surfaces

Investigations for applying the impedance surface in horn antennas for radiation pattern control have been conducted by many researchers[9,10,11]. The introduction of the lossy material on the inner walls of the horn antenna provides a good potential for the replacement of corrugations. However, the coating of lossy material introduces ohmic losses ranging in gain losses of 0.5 dB in [9], 10 dB in[10], and 0.8-2.7 dB in [11]. Our goal for using impedance surfaces is to control the horn antenna radiation pattern at a minimum ohmic loss. Such a goal can be achieved by a comprehensive study of the coating on the inner walls of a horn antenna.

Based on the stepped waveguide mode outlined in Figure 1, the ohmic loss is mainly contributed by the imaginary part of the propagation constant of the dominant mode (HE_{11}) along the horn transition. Further studies of the eigenvalue of the dominant mode (HE_{11}) suggest that the ohmic losses depend upon the material

properties, the thickness of the coating, and the size of waveguide cross section. The following **design guidelines** hightlight the importance of each factor:

- As was noted in [10], the ohmic losses decrease monotonically as the cross-sectional size increases because the electromagnetic fields are expelled from the lossy material when the cross-sectional size of the horn transition is large. This explains why the antenna in [9] has significantly smaller ohmic losses than others. One can reduce the ohmic losses by not applying the lossy coating on the small cross-sectional portion of the horn transition while applying a robust coating on the large cross-sectional portion of the horn.

- For a large cross-sectional size antenna, the choice of the material is less critical. For a smaller size antenna, choice of the lossy material is more important to achieve the needed HE_{11} mode in the horn transition. A good material for such an application is one having a high magnetic loss.

- There exists an optimum thickness of the lossy material coating for low-loss implememtation of the HE_{11} mode.

Experimental results presented in a later section demonstrate a significant reduction of ohmic loss by following the above design guidelines.

D. Pattern Synthesis with Numerical Optimizations

A study of a more feasible method for the horn antenna pattern synthesis using impedance surfaces has been conducted. It is found that a reliable and practical theoretical design can be performed by using numerical optimization of the error function. The error function is constructed based on the difference between the

desired aperture eigenmodes and the eigenmodes resulted from analytical solution of the horn transition and the outer aperture. The control parameters are the total length of the impedance coating, the thickness of the sheet in different section of the horn transition, and the frequency sample points in the desired antenna operating frequency band. More explicitly, the error function can be expressed as:

$$Err(\ell, \mathbf{h}, \mathbf{f}) = \sum_{f_i} \left\{ |\mathbf{A}_{desired} - \mathbf{A}_{design}(\ell, \mathbf{h}, f_i)|^2 + |S_{11}^T(\ell, \mathbf{h}, f_i)|^2 \right\} \qquad (53)$$

where $\mathbf{h} = (h_1, h_2, ...)$, $\mathbf{A}$'s are the relative amplitude sets of the eigen modes, and S_{11}^T is the reflection coefficient of in the feeding waveguide. The error function $Err(\ell, \mathbf{h}, \mathbf{f})$ is then minimized with respect to the parameters by using a Fletcher-Powell numerical optimization process[12,13]. Similar design processes have been applied to optimize the structure designs of a microwave double-plane transformer[5] and of a horn antenna on a ground plane[6]. Both applications have demonstrated that the optimization process is an effective computer-aided design tool.

II. RESULTS

At the beginning of this research period, in order to identify the source of the rapid variant ripples in the backlobe of the H-plane radiation pattern, a two-dimensional horn model, having the same profile as that of the 20-dB standard gain pyramidal horn in the principal H-plane, was introduced to investigate the effects of the electric current on the outer surfaces of the horn. Since a two-dimensional model requires significantly less unknowns than a three-dimensional model, the two-dimensional moment method solution permits the use of sufficiently small segment size to obtain results which compare well with measurements. Figure 3 shows the comparison of

the measured and predicted (based on the two-dimesional model) radiation patterns of the 20-dB standard gain pyramidal horn with PEC walls at a frequency of 10.1 GHz. As we can see from the figure, when the outer surfaces and the feeding structure are included in the moment method solution, the two-dimensional horn model predicts quite well the radiation pattern and its rapid variant pattern structures, except the very last few ripples. These outer most lobes are influenced by the spilled-over energy from the E-plane section of the pyramidal horn that the two-dimensional H-plane horn does not model. This study lead us to believe that the source of the quick variant ripples is the induced electric current on the outer surfaces of the horn antenna. If all the ripple structures of the radiation patterns, both in the E- and H-plane of the pyramidal horn are to be analyzed and controlled accurately, the entire outer surface of the pyramidal horn has to be included in the moment method solution. It is through this investigation that we have decided to include the entire outer surfaces, or at least a big portion, of the pyramidal horn antenna in the moment method solution to provide a more accurate analysis and the pattern control.

Based on the analysis method of stepped waveguides with impedance surface presented in this report, design curves for different thicknesses of coated material are computed to show how ohmic losses are affected by the coated material thickness and the size of the rectangular cross-section of the horn. Typical curves are shown in Figure 4 for a Northrop Nitrile lossy magnetic material which has a relative permitivity of $18.75 - j0.1$ and a relative permeability of $1.55 - j1.85$ at 10 GHz. The design curves indeed show an optimum coating thickness, for minimum ohmic loss, of 60-mils for the given material at 10 GIIz for horn transitions with cross-sections ranging from 1 to 7 inches.

To validate the analysis of the horn transition and the design guidelines of horns

with low losses using impedance surfaces, two square aperture horns were constructed. The smaller horn has dimensions of 5 inches by 5 inches on the aperture, and 10.5 inches in length. The larger one has 7 inches by 7 inches on the aperture, and 12.2 inches in length. Following the design guidelines suggested previously and the data of Figure 4, the 60-mil Northrop Nitrile sheet material leads to the smallest ohmic losses. Because of the unavailability to us of that thickness of the material, a 40-mils thickness was chosen to demonstrate the method. The coating length of the material was chosen to those included in a previous report which also used the same length of material coating but had slightly different thickness of Eccosorb-GDS which has a relative permitivity of $14.83 - j0.06$ and a relative permeability of $1.47 - j1.46$.

The measured E-plane patterns based on the the new design guidelines for the horns are shown in Figures 5 and 6 for the horns with square apertures. It can be noted that the gain loss of the smaller horn using the Northrop Nitrile material is 1.75 dB while the gain loss for the larger horn using the same material is only 0.24 dB. In a previous progress report, it was indicated that using Eccosorb-GDS material of the same length of coating, the gain loss on a 20-dB standard gain horn, which had 3.62 inches E-plane aperture size, resulted in about 4.5 dB gain loss which is far greater than either one of the new designs. It is apparent that the new method of analysis and design quidelines do lead to horn designs with impedance surfaces with far smaller ohmic losses.

III. FUTURE WORK

After the progress during this period, the research project is now based on a more sound theoretical technique. We will concentrate our future work on integrating

the developed techniques for the analysis, synthesis, and control of horn antenna radiation patterns using impedance surfaces with low horn gain losses.

References

[1] H. Flügel and E. Kühn, "Computer-aided analysis and design of circular waveguide tapers," *IEEE Trans. Microwave Theory Tech.*, vol. MTT-36, pp. 332–336, Feb. 1988.

[2] F. Sporleder and H.-G. Unger, *Waveguide tapers and couplers.* Peter Peregrinus Ltd., London, 1979.

[3] E. Kühn and V. Hombach, "Computer-aided analysis of corrugated horns with axial or ring-loaded radial slots," *Proc. ICAP 83 part 1*, pp. 127–131, 1983.

[4] J. A. Encinar and J. M. Rebollar, "A hybrid technique for analyzing corrugated and noncorrugated rectangular horns," *IEEE Trans. Antennas Propagat.*, vol. AP-34, pp. 961–968, Aug. 1986.

[5] H. Patzelt and F. Arndt, "Double-plane steps in rectangular waveguides and their application for transformers, irises, and filters," *IEEE Trans. Microwave Theory Tech.*, vol. MTT-30, pp. 771–776, May 1982.

[6] T. Wriedt, K. H. Wolff, F. Arndt, and U. Tucholke, "Rigorous hybrid field theoretic design of stepped rectangular waveguide mode converters including the horn transitions into half-space," *IEEE Trans. Antennas Propagat.*, vol. AP-37, pp. 780–790, June 1989.

[7] S. I. Ghobrial and H. R. Sharobim, "Radiation patterns of paraboloidal reflector fed by a pyramidal horn with lossy walls," *IEEE Trans. Antennas Propagat.*, vol. AP-37, pp. 1316–1317, Oct. 1989.

[8] C. A. Balanis, *Advanced Engineering Electromagnetics.* Wiley, 1989.

[9] C. M. Knop, Y. B. Cheng, and E. L. Ostertag, "On the fields in a conical horn having an arbitrary wall impedance," *IEEE Trans. Antennas Propagat.*, vol. AP-34, pp. 1092–1098, Sept. 1986.

[10] C. S. Lee, S. W. Lee, and D. W. Justice, "A simple circular-polarized antenna: Circular waveguide horn coated with lossy magnetic material," *IEEE Trans. Antennas Propagat.*, vol. AP-36, pp. 297–299, Feb. 1988.

[11] J. J. H. Wang, V. K. Tripp, and J. E. Tehan, "The magnetically coated conducting surface as a dual conductor and its application to antennas and microwaves," *IEEE Trans. Antennas Propagat.*, vol. AP-39, pp. 1069–1077, July 1990.

[12] F. R. and M. J. D. Powell, "A rapidly convergent descent method for minimization," *Computer Journal*, vol. 6, pp. 163–168, 1963.

[13] W. H. Press, B. P. Flannery, S. A. Teukolsky, and W. T. Vetterling, *Numerical Recipes.* Cambridge University Press, 1986.

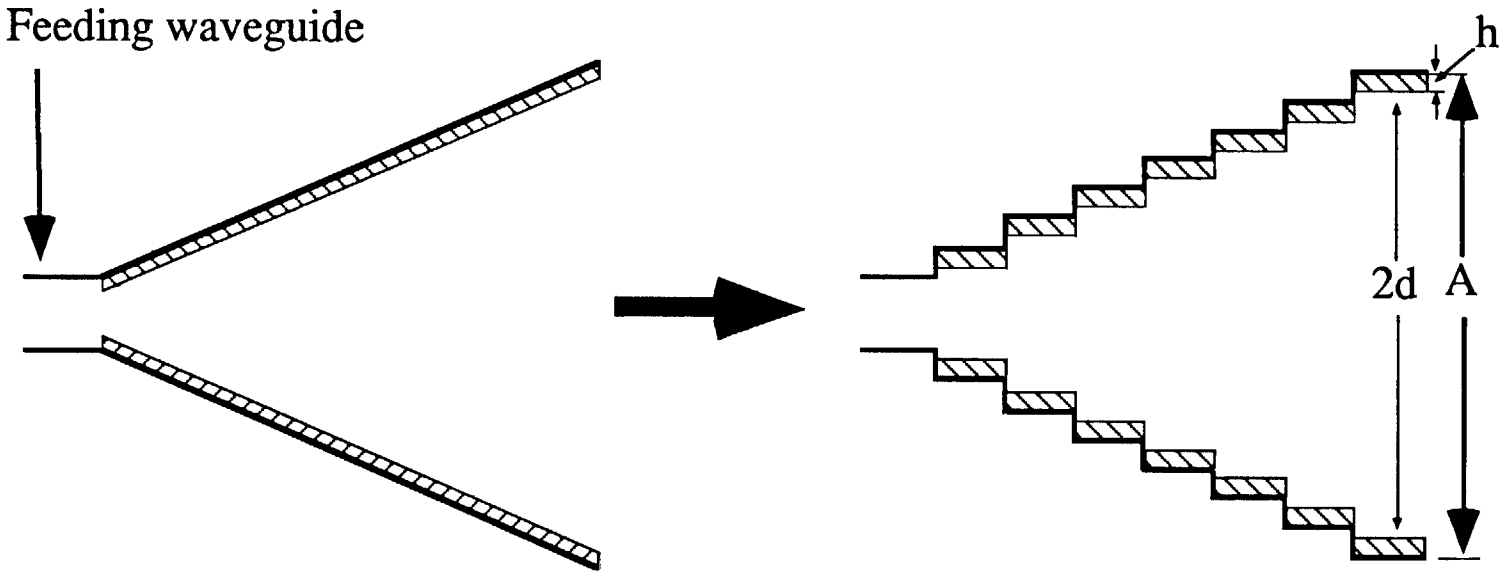

Figure 1. Stepped-waveguide model for a horn transition with impedance surfaces.

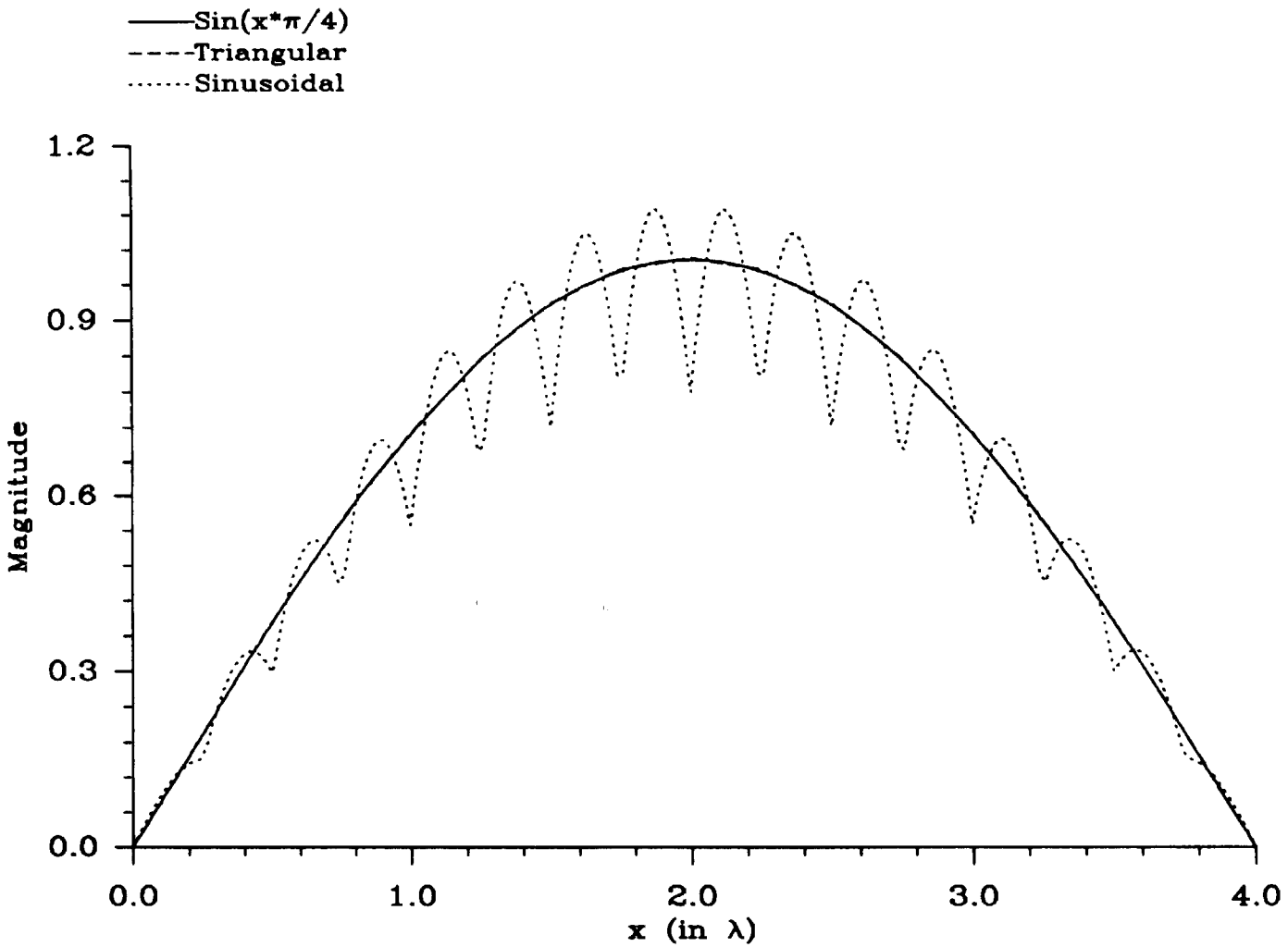

Figure 2. Comparison of accuracies by using subsectional sinusoidal and triangular functions to represent the function Sin(x*π/4).

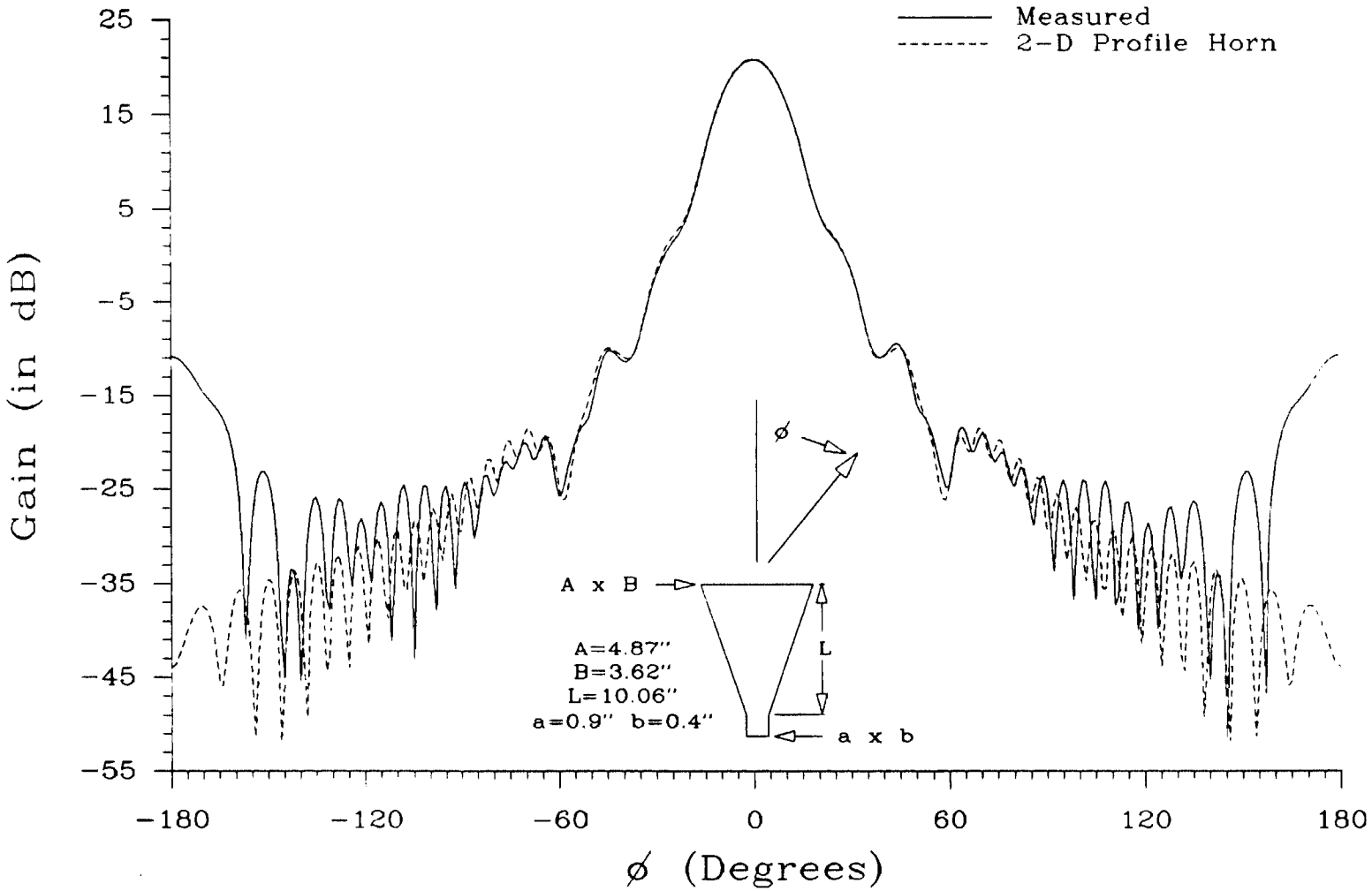

Figure 3. H-plane gain pattern for 20-dB horn with PEC walls at 10.1 GHz.

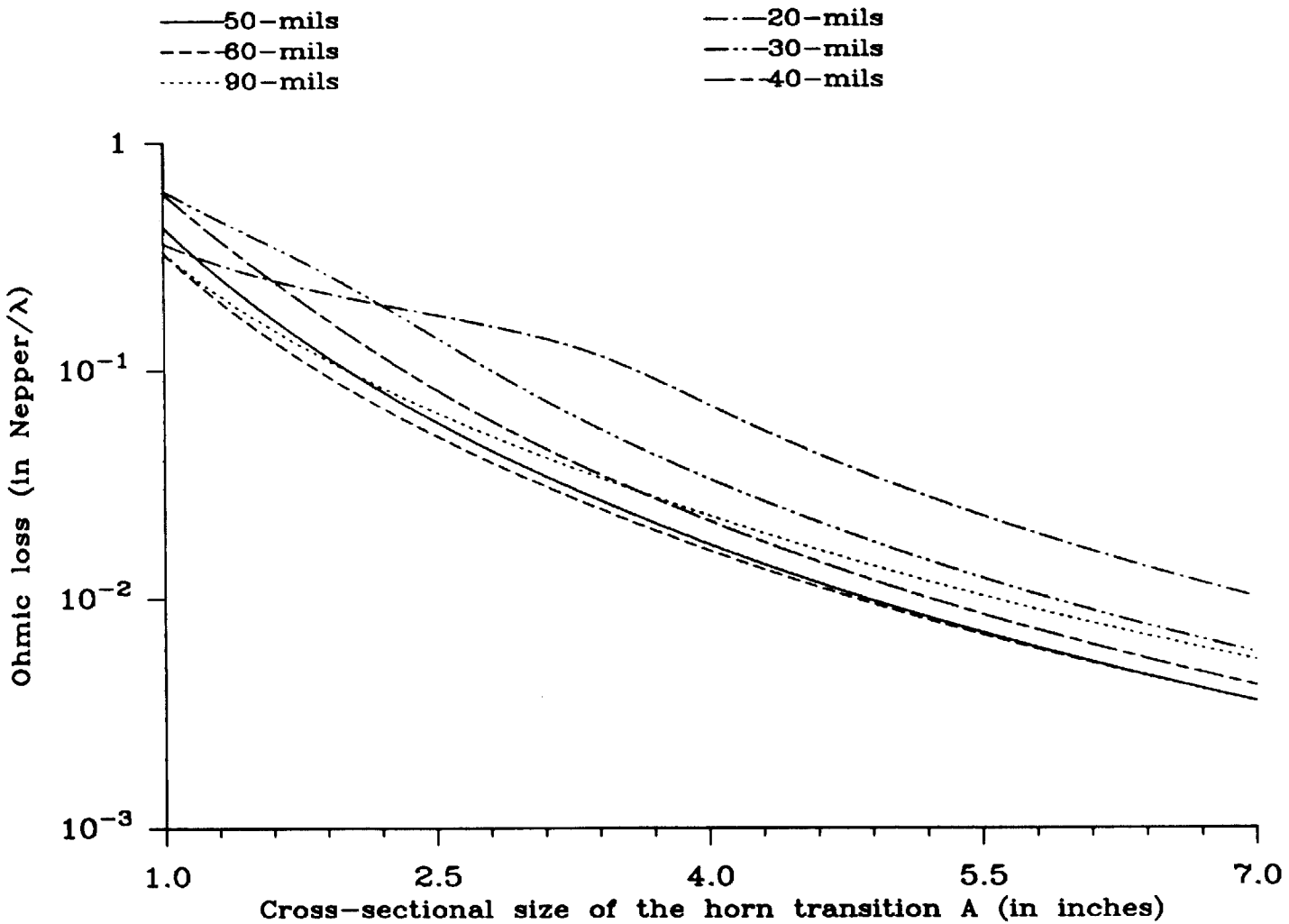

Figure 4. Ohmic loss design curves for different lossy material coating thicknesses at 10 GHz.

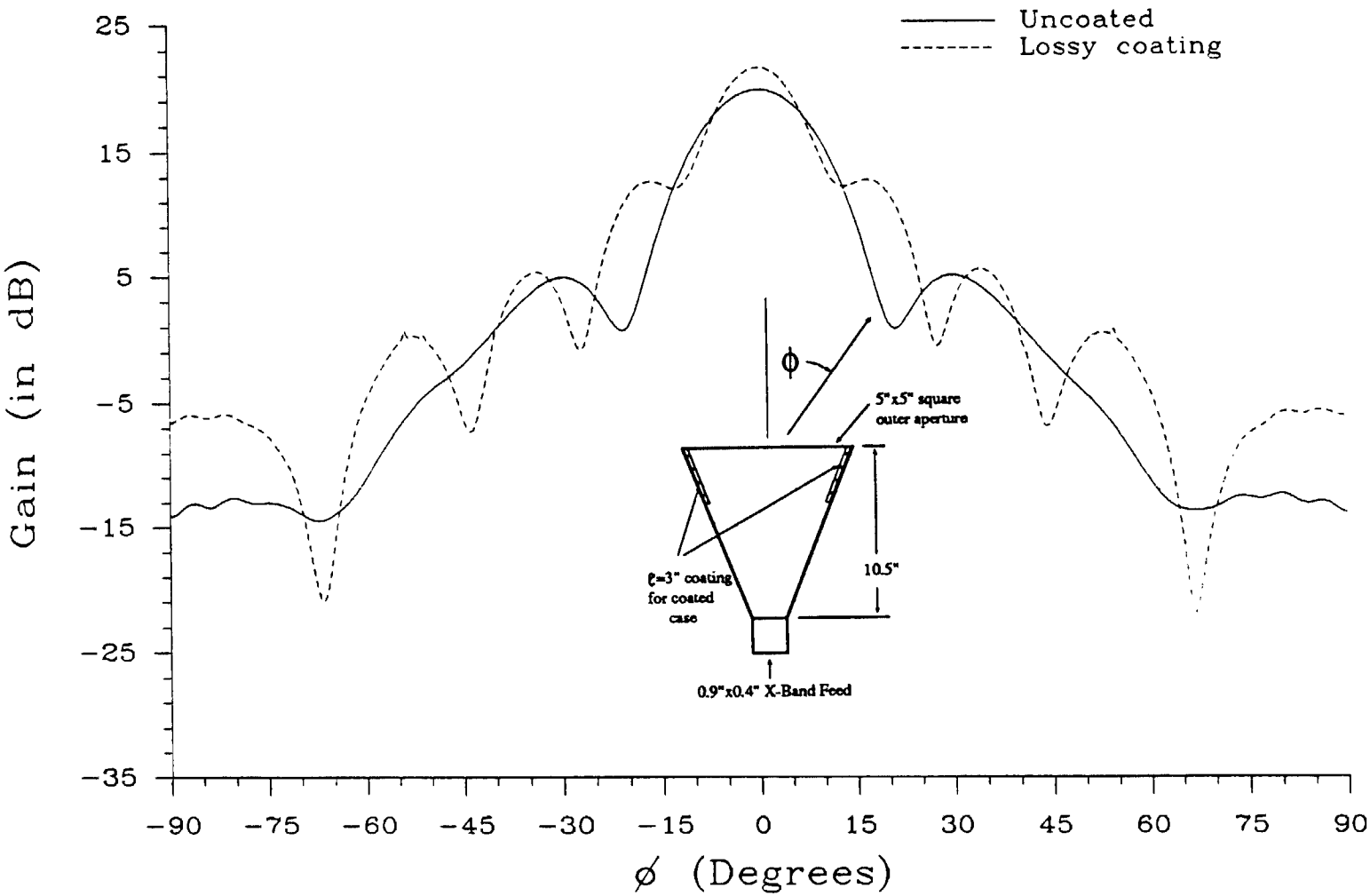

Figure 5. Comparison between coated and uncoated E-plane measured patterns of a 5-in square aperture horn.

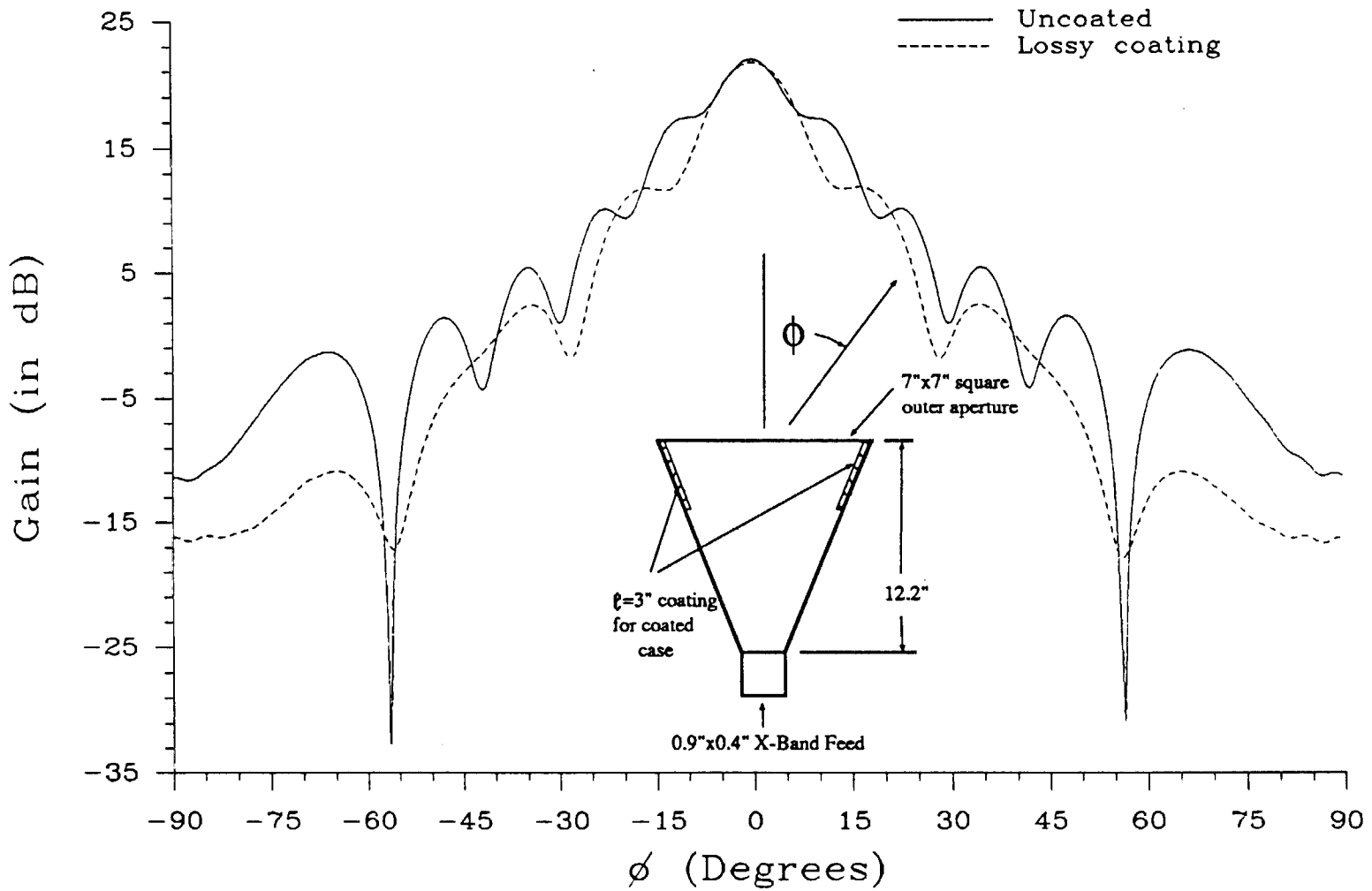

Figure 6. Comparison between coated and uncoated E-plane measured patterns of a 7-in square aperture horn.